Accepted Manuscript

A methodology for hybrid simulation of Rarefield and continuum flow regimes

Foluso Ladeinde, Xiaodan Cai, Ramesh Agarwal

PII: S1270-9638(17)31641-3
DOI: https://doi.org/10.1016/j.ast.2017.12.036
Reference: AESCTE 4370

To appear in: *Aerospace Science and Technology*

Received date: 6 September 2017
Revised date: 17 December 2017
Accepted date: 18 December 2017

Please cite this article in press as: F. Ladeinde et al., A methodology for hybrid simulation of Rarefield and continuum flow regimes, *Aerosp. Sci. Technol.* (2018), https://doi.org/10.1016/j.ast.2017.12.036

A Methodology for Hybrid Simulation of Rarefield and Continuum Flow Regimes

By

Foluso Ladeinde
Mechanical Engineering Department
SUNY Stony Brook
Stony Brook, NY 11794-2300

Xiaodan Cai[†]
TTC Technologies, Inc.
Centereach, NY 11720

Ramesh Agarwal
Mechanical and Aerospace Engineering Department
Washington University in St. Louis
St. Louis, MO 63130

A hybrid procedure consisting of a high order continuum (HOC) model and the direct simulation Monte-Carlo (DSMC) solver is proposed in this paper, as it represents a promising approach for seamless computation of hypersonic flows in all regimes. This approach also allows the effects of thermophysics (thermal and chemical non-equilibrium) and turbulence to be included so that gas interactions can be modeled much more easily than in other approaches. Such hybrid procedures can also be developed into robust and efficient parallel computing tools for practical 3D computations. The main idea behind the proposed HOC/DSMC methodology consists of incorporating the physically realizable and computationally stable version of the Burnett equations into hypersonic codes that have the capability for calculating non-equilibrium chemistry and temperature. We explore the feasibility of simplified, yet accurate and numerically

stable, versions of the Burnett equations. We discuss such a model in detail, providing an analysis of its stability and performance for Alsmeyer's shock wave problem and hypersonic flow over a sphere. We also report on the performance of the DSMC component of the proposed hybrid scheme.

[†]Current Affiliation: United Technologies Research Center (UTRC), East Hartford, CT, USA

Nomenclature

Y_s	Mass concentration of species s
D_s	Effective diffusion coefficient for Species s, m^2/s
D_{sk}	Multicomponent diffusion coefficient
e	Elementary electronic charge, 1.6022×10^{-19} C or total energy per unit mass
E	Electronic field, function(space, time), V/m
E_e	Electronic translational energy per unit volume
ϵ_o	Permittivity of free space, 8.8542×10^{-12}, F/m
h^o	Enthalpy of formation
k	Boltzmann constant, 1.3807×10^{-23} J/K
L	Characteristic length
M_e	Electron mass, 9.1094×10^{-31} kg
M	Mach number, Molecular weight
N	Number density
p	Pressure

q	Charge, C, or heat flux vector
Q_{rad}	Radiation heat loss term
Q	Energy exchange between modes
T	Translational temperature
T_v	Vibrational temperature
u^j	Mass-averaged velocity component in 3 dimensions, m/s, j=1 to 3
u_s	Average or mean velocity
V	Random or peculiar velocity or diffusion velocity
Z_s	Ionic valency, -1 for electrons, 1 for single-ionized positive ions
τ	Relaxation time
τ^{ij}	Viscous shear stress
x^j	Position vector in 3 dimensions, j=1 to 3
X	Mole fraction
ν	Collision frequency
ν^*_{er}	Effective collision frequency of electrons with diatomic molecules (heavy particles)
Θ_d	Characteristic temperature of dissociation
Θ_v	Characteristic temperature of vibration
Γ	Flux density
ω_{pe}	Electron plasma frequency, 5.64×10^4 rad/s
ω	Source or sink of species
η'	Thermal conductivity coefficient
σ	Collision cross-section

ρ_n State density in the n^{th} vibrational level

ρ Total density, kg/m^3

Subscripts

D Debye

e Electron

I Ion

n,m Species indices in quantum level

R Diatomic molecule (heavy particle)

s Species

v Vibration

∞ Freestream conditions

Superscripts

i, j i^{th} and j^{th} components in general orthogonal coordinates

INTRODUCTION

Hypersonic flows over space vehicles produce flow fields with local Knudsen numbers, *Kn*, which may lie in all the three regimes – continuum, transition, and rarefied. The Navier-Stokes (NS) equations and the direct simulation Monte-Carlo (DSMC) methods can accurately and efficiently model the flows in the continuum and rarefied regimes, respectively. Of these two approaches, i.e., continuum and kinetic, the latter considers an ensemble of small particles or molecules whose distribution function can be determined as a solution of the Boltzmann equation. The former approach is based on the representation of the gas as a fluid continuum governed by

the mass, momentum, and energy conservation laws. Although, theoretically, the kinetic approach is appropriate for simulating gas flows in any regime; in practice, it can require prohibitively large computational resources if the gas flow is dense. DSMC remains an efficient numerical technique for solving the Boltzmann equation [1]. It enables the computation of flows with Knudsen numbers $Kn \geq 0.001$ for 2D problems and $Kn \geq 0.01$ in the 3D case, i.e., almost nearly down to the continuum regime [2,3]. (Of course, these Kn values, 0.001 and 0.01, are approximate.) Here, $Kn = \lambda/L$, where λ is the mean free path of the molecules and L is the characteristic length scale of the flow. Nevertheless, DSMC computations are still too expensive in many cases, especially for 3D engineering applications. Also, being a rather efficient tool for supersonic and particularly hypersonic flows [3], they become more resource-consuming for low Mach number subsonic flows, due to difficulties with boundary condition implementation on subsonic inflow/outflow boundaries [4]. Furthermore, obtaining gas interactions with DSMC is a difficult task. The continuum approach is much cheaper and more versatile in these regards. There is, therefore, a strong motivation for its utilization at the low Kn values.

The traditional continuum model is based on the Navier-Stokes equations, which are the first order approximation to the Boltzmann equation with respect to Kn as the small parameter in the asymptotic expansion. Coupled with no velocity slip/no temperature jump solid wall boundary conditions, they are valid if the Knudsen number is smaller than 0.001. More rarefied flows should be described using the Navier-Stokes equations with velocity slip/temperature jump boundary conditions. However, the flows in the transitional regime ($0.1 < Kn < 10$) require higher order models, the most well-known being the Burnett equations obtained as second order approximations with respect to Kn. Though there are some difficulties with the stability of their solutions and the development of relevant solid wall boundary conditions, recent enhancements [5] allow the consideration of the (modified) Burnett equations as a potential continuum model

for transitional flows. In recent years, Burnett equations have been successfully employed to compute 3D hypersonic flows in continuum-transition regimes [6], although it has been difficult to compute flows for $Kn>1$ with the approach.

The other HOC equations, such as Eu's [7] and Grad's 13-moment equations [8], are significantly more expensive to compute than the Burnett equations, and have been tested only for 1D and for 2D geometrically simple problems. Another approach is due to Aristov and Tcheremissin [9], wherein a special quadrature formula is employed for the collision integral on the right-hand side. This method has been applied to solve 2D problems involving a mono-atomic gas. Application of the approach to gases with internal degrees of freedom is problematic at the moment, given the difficulty with the inclusion of chemical reactions.

A detailed description of the DSMC method and the direct Boltzmann solver of Aristov and Tcheremissin, as well as the discussions of their relative advantages and disadvantages, can be found in the references. However, none of the approaches can efficiently compute all the flow regimes that may be present on a space vehicle in hypersonic flight.

A careful examination of the options has led us to the conclusion that a hybrid high order continuum/direct simulation Monte-Carlo (HOC/DSMC) solver represents the most promising approach for seamless computation of hypersonic flows in all regimes. Moreover, the procedure can easily be extended to include the effects of thermophysics (thermal and chemical non-equilibrium) and turbulence. In addition, the proposed hybrid codes can be developed to be robust, stable, and efficient on parallel computing platforms for practical 3D computations. The main idea behind the proposed HOC/DSMC methodology is described below.

The hybrid method requires for each cell: (a) the determination of which approach – continuum or particle - is valid, and: (b) the development of interface boundary conditions, which basically connect the two approaches at the cell interface. For each cell, whether the continuum model breaks down or not is determined by employing a switching (or breakdown) parameter. There are a few switching criteria that have been proposed in the literature [10,11], each of which is based on the premise that the Navier-Stokes equations are not valid when the nonlinear terms in the Chapman-Enskog expansion become important - when the velocity distribution function deviates from its equilibrium state by some degree. One can use the criteria based either on the local Knudsen number or on the ratio of the maximum shear stress to the maximum heat-flux. However, the effectiveness of various possible criteria needs to be evaluated by numerical experiments. Limited amount of work has been carried out on this issue, but see Boyd [12] for a short review of breakdown prediction. In the present study, the gradient-length-local Knudsen number discussed by Boyd has been used, although other options, such as the parameter involving direct evaluation of heat flux tensor elements, have also been tested.

Once the cells in which the continuum model holds have been identified using the switching criteria, the calculations for the rest of the cells in the flow field are performed with the DSMC method. The next important issue in the hybrid method is connecting the continuum cells with the particle cells on the interface in a seamless fashion. On one hand, the numerical fluxes calculated by the continuum approach must be transformed into particle fluxes for the DSMC method. On the other, the field values of macroscopic quantities such as density, velocity, pressure, and temperature must be calculated from the ensemble in the particle simulation cells in the vicinity of the continuum cells, since these values are needed for calculating the numerical fluxes in the continuum scheme. For the DSMC method, we need to know the particle velocity distribution function at the cell interface. This distribution function, which can be Maxwellian, Navier-Stokes, or Burnett, requires the knowledge of the macroscopic density, bulk velocity, and temperature

from the continuum cell for Maxwellian, as well as the gradients of the macroscopic quantities, for Navier-Stoke; and the mixed gradients, for the Burnett distribution functions. This procedure can be performed in a reverse order as well by first carrying out the DSMC computations and then using the particle distribution functions from DSMC to compute the numerical fluxes for the bordering continuum cells.

Both the NS and Burnett shear stress and heat flux tensors in the switching condition are implemented in the current procedure, as are the NS and Burnett distribution functions at the interface of the particle and continuum cells. Although it has been established conclusively that the Burnett equations give more accurate results compared to the Navier-Stokes equations [13, 14], the results must be re-established within the context of non-equilibrium models. Therefore, we are testing the relative merits of using NS versus Burnett shear stress and heat flux tensors and distribution functions in the hybrid technique by analyzing a 1D model problem to ensure that the method is robust (stable) for non-equilibrium problems. Various boundary conditions associated with velocity slip, temperature slip and catalytic surface are formulated for the hybrid solver. Several test cases for the hybrid solver are considered, including the shock wave problem of Alsmeyer [15] and the computation of hypersonic flow in the vicinity of a sharp leading edge (~ 100 to 300λ). The latter problem is especially challenging since the flow passes through the different regimes, from free molecular to continuum, via transitional mode. An even more challenging problem will be an accurate simulation of the interaction of hypersonic boundary layers with shock waves. Disagreement between the predicted length of the separation zone by the NS and DSMC codes has been reported. Note that no one has previously reported on the simulations of this problem with the Burnett models.

The procedure in this paper combines the Burnett equations with both thermal and chemical nonequilibrium models, which are based on the LAURA [16] code from NASA Langley. We

have added the Burnett and rotational temperature equations to LAURA, since the code, being limited to translational and vibrational temperatures, did not have these capabilities. The option for the complete 11-species equations (or subsets thereof) for chemical nonequilibrium is also supported in the present procedure. The species-specific equations for the vibrational energy, such as in Josyula and Bailey [17] have also been solved in our work. The addition of turbulence models into the present framework is obviously a straightforward task and will be reported in subsequent work. The DSMC component of the proposed hybrid scheme has been developed in-house.

The governing equations in our code are presented in the following two sections, including a simplified version of the Burnett equations, courtesy of Lumpkin [13]. We then discuss the solution methodologies and the parameter space for the computation of Alsmeyer's shock wave problem and hypersonic flow over a sphere, which are the two problems we report on in this paper. An appendix is provided on the coefficients that appear in the BGK Burnett equations.

GOVERNING EQUATIONS

The governing equations for the HOC component of the hybrid procedure can be written as follows:

Species Conservation:

$$\frac{\partial}{\partial t}\rho_s + \frac{\partial}{\partial x^j}\rho_s u^j = \frac{\partial}{\partial x^j}\left(\rho D_s \frac{\partial}{\partial x^j} y_s\right) + \dot{\omega}_s \tag{1}$$

Mixture Momentum Conservation:

$$\frac{\partial}{\partial t}\rho u^i + \frac{\partial}{\partial x^j}\rho u^i u^j = -\frac{\partial p}{\partial x^i} + \frac{\partial}{\partial x^j}\left(\mu\left(\frac{\partial u^i}{\partial x^j} + \frac{\partial u^j}{\partial x^i}\right) - \frac{2}{3}\mu\frac{\partial u^i}{\partial x^i}\delta^{ij}\right) + \frac{\partial \tau_{ij}^B}{\partial x^j} + \sum_s ne_s Z_s E^i$$

(2)

Vibrational Energy Conservation (average):

$$\frac{\partial}{\partial t}\rho e_v + \frac{\partial}{\partial x^j}\rho e_v u^j = \frac{\partial}{\partial x^j}\left(\eta_v \frac{\partial T_v}{\partial x^j}\right) + \frac{\partial}{\partial x^j}\left(\rho\sum_{s=1}^{11} h_{v,s} D_s \frac{\partial y_s}{\partial x^j}\right) + \sum_{s=mol.} \rho_s \frac{\left(e^*_{v,s} - e_{v,s}\right)}{\langle\tau_s\rangle} + \sum_{s=mol.} \rho_s \frac{\left(e^{**}_{v,s} - e_{v,s}\right)}{\langle\tau_{es}\rangle} + \sum_{s=mol.} \dot{\omega}_s \hat{D}_s \quad (3)$$

Vibrational Energy Conservation (multi-component):

$$\frac{\partial}{\partial t}\rho_s e_{v,s} + \frac{\partial}{\partial x^j}\left(\rho_s e_{v,s} u^j\right) = \frac{\partial}{\partial x^j}\left(\eta'_{v,s}\frac{\partial T_v}{\partial x^j}\right) - \frac{\partial}{\partial x^j}\left(\rho_s e_{v,s} V_s^j\right) + \rho_s \frac{\left(e^*_{v,s} - e_{v,s}\right)}{\langle\tau_s\rangle}\left(\equiv Q_{T-V}\right)$$

$$+ N_e \frac{\left(e^*_{v,s}(T_e) - e_{v,s}\right)}{\tau_{es}}\left(\equiv Q_{e-V}\right) + \dot{\omega}_s D_s \quad (4)$$

Electron and Electronic Excitation Energy Conservation:

$$\frac{\partial}{\partial t}\rho e_e + \frac{\partial}{\partial x^j}\left[\left(\rho e_e + p_e\right)u^j\right] = u^j\frac{\partial p_e}{\partial x^j} + \frac{\partial}{\partial x^j}\left(\eta_e\frac{\partial T_e}{\partial x^j}\right) + \frac{\partial}{\partial x^j}\left(\rho\sum_{s=1}^{11} h_{e,s} D_s \frac{\partial y_s}{\partial x^j}\right) + 2\rho_e\frac{3}{2}\overline{R}(T - T_e)\sum_{s=1}^{10}\upsilon_{es}/M_s - \sum_{s=6}^{10}\dot{n}_{e,s}\hat{I}_s - \sum_{s=mol.}\rho_s\frac{\left(e^{**}_{v,s} - e_{v,s}\right)}{\langle\tau_{es}\rangle} - Q_{rad} \quad (5)$$

Rotational Energy Conservation:

$$\frac{\partial}{\partial t}\rho e_r + \frac{\partial}{\partial x^j}\left(\rho e_r u^j\right) = \left(\frac{\partial}{\partial x^j}\left(\eta_r\frac{\partial T_r}{\partial x^j}\right)\right)^j + \frac{\partial}{\partial x^j}\left(\rho\sum_{s=1}^{11} h_{r,s} D_s\frac{\partial y_s}{\partial x^j}\right) + \frac{\rho c_{vr}(T - T_R)}{\tau_{rt}} \quad (6)$$

Translational Energy Conservation:

$$\frac{\partial}{\partial t}\rho e_t + \frac{\partial}{\partial x^j}\rho e_t u^j = -p\frac{\partial u^i}{\partial x^i} - \tau_{ij}\frac{\partial u^i}{\partial x^j} + \frac{\partial}{\partial x^j}\left(\eta_t \frac{\partial T_v}{\partial x^j}\right) + \frac{\partial}{\partial x^j}\left(\rho\sum_{s=1}^{11} h_{t,s} D_s \frac{\partial y_s}{\partial x^j}\right)$$
$$-\frac{\rho c_{vr}(T - T_R)}{\tau_{rt}} - \sum_{s=1}^{11}\rho_s \frac{\left(e^{**}{}_{v,s} - e_{v,s}\right)}{\langle \tau_s \rangle} \qquad (7)$$

Total Energy Conservation

$$\frac{\partial}{\partial t}\rho E + \frac{\partial}{\partial x^j}\rho H u^j = \frac{\partial}{\partial x^j}\left(\eta\frac{\partial T}{\partial x^j} + \eta_v\frac{\partial T_v}{\partial x^j} + \eta_r\frac{\partial T_r}{\partial x^j} + \eta_e\frac{\partial T_e}{\partial x^j}\right) + \frac{\partial q_i^B}{\partial x^j} + \frac{\partial}{\partial x^j}\left(\rho\sum_{s=1}^{11} h_s D_s \frac{\partial y_s}{\partial x^j}\right)$$
$$+\frac{\partial}{\partial x^j}\left(u^i\mu\left(\frac{\partial u^i}{\partial x^j} + \frac{\partial u^j}{\partial x^i}\right) - \frac{2}{3}u^i\mu\frac{\partial u^k}{\partial x^k}\delta^{ij}\right) - Q_{rad} \qquad (8)$$

The reader should consult the nomenclature section in this paper and also Gnoffo et al. [16] for the various symbols in these equations. Note that the τ_{ij}^B term in the momentum equations refers to the additional stress tensor (in the BGK Burnett equations) over that for the Navier-Stokes equations. Similarly, q_i^B refers to the additional heat flux vector. The subscript "s" represents the species component, "v" represents the vibrational mode and "e" for the electrons. We include 11 species in the modeled system. Species 1 to 5 are the neutral components of air consisting of N, O, N_2, O_2, and NO. Species 6 to 10 are the ions corresponding to species 1 to 5, in which one electron has been removed. Species 11 are the free electrons. It is important to note that only the translational and vibrational energies are included in the HOC calculations for the present results. Moreover, the vibrational energy equation is calculated in the average form in this paper, with the decision to focus on the extensively validated two-temperature model [12], wherein it is assumed that the distribution of energy in both the vibrational and electronic modes can be described by a single temperature. The two-temperature models are thus used to fit the thermodynamic property curves for the 11 species, the collision cross sections, the transport properties, the chemical kinetic models, and the vibrational and electronic energy relaxation models. The model details for

physical processes such as the translational-vibrational (T-V) energy exchange and electron-vibrational energy exchange appearing in Eqn. (3) and (4) etc., are described elsewhere [17, 18].

The BGK Burnett Equations

The physically realizable and computationally convergent version of the Burnett equations[18] is used in our HOC procedure; and is shown below. Note that the linear – with respect to the Chapman-Enskog expansion - (Navier-Stokes) terms, denoted by superscript "(1)," are also shown below. The values of the constants in the equations are given in the appendix.

$$\sigma_{11}^{(1)} = -\mu(\tfrac{4}{3}u_x - \tfrac{2}{3}v_y - \tfrac{2}{3}w_z)$$

$$\sigma_{22}^{(1)} = -\mu(\tfrac{4}{3}v_y - \tfrac{2}{3}w_z - \tfrac{2}{3}u_x)$$

$$\sigma_{33}^{(1)} = -\mu(\tfrac{4}{3}w_z - \tfrac{2}{3}u_x - \tfrac{2}{3}v_y)$$

$$\sigma_{12}^{(1)} = \sigma_{21}^{(1)} = -\mu(u_y + v_x)$$

$$\sigma_{23}^{(1)} = \sigma_{32}^{(1)} = -\mu(v_z + w_y)$$

$$\sigma_{31}^{(1)} = \sigma_{13}^{(1)} = -\mu(w_x + u_z)$$

$$q_1^{(1)} = -\kappa T_x$$

$$q_2^{(1)} = -\kappa T_y$$

$$q_3^{(1)} = -\kappa T_z$$

The Burnett terms are given below:

$$\sigma_{11}^{(2)} = \frac{\mu^2}{p}\Big(\alpha_1 u_x^2 + \alpha_2 u_y^2 + \alpha_3 u_z^2 + \alpha_4 v_x^2 + \alpha_5 v_y^2 + \alpha_6 v_z^2 + \alpha_7 w_x^2 + \alpha_8 w_y^2 + \alpha_9 w_z^2 + \alpha_{10} u_x v_y$$

$$+ \alpha_{11} v_y w_z + \alpha_{12} w_z u_x + \alpha_{13} u_y v_x + \alpha_{14} v_z w_y + \alpha_{15} w_x u_z + \alpha_{16} RT_{xx} + \alpha_{17} RT_{yy} + \alpha_{18} RT_{zz}$$

$$+ \alpha_{19} \frac{RT}{\rho} \rho_{xx} + \alpha_{20} \frac{RT}{\rho} \rho_{yy} + \alpha_{21} \frac{RT}{\rho} \rho_{zz} + \alpha_{22} \frac{RT}{\rho^2} \rho_x^2 + \alpha_{23} \frac{RT}{\rho^2} \rho_y^2 + \alpha_{24} \frac{RT}{\rho^2} \rho_z^2 + \alpha_{25} \frac{R}{T} T_x^2$$

$$+ \alpha_{26} \frac{R}{T} T_y^2 + \alpha_{27} \frac{R}{T} T_z^2 + \alpha_{28} \frac{R}{\rho} T_x \rho_x + \alpha_{29} \frac{R}{\rho} T_y \rho_y + \alpha_{30} \frac{R}{\rho} T_z \rho_z \Big)$$

$$\sigma_{22}^{(2)} = \frac{\mu^2}{p}\Big(\alpha_1 v_y^2 + \alpha_2 v_z^2 + \alpha_3 v_x^2 + \alpha_4 w_y^2 + \alpha_5 w_z^2 + \alpha_6 w_x^2 + \alpha_7 u_y^2 + \alpha_8 u_z^2 + \alpha_9 u_x^2 + \alpha_{10} v_y w_z + \alpha_{11} w_z u_x$$

$$+ \alpha_{12} u_x v_y + \alpha_{13} v_z w_y + \alpha_{14} w_x u_z + \alpha_{15} u_y v_x + \alpha_{16} RT_{yy} + \alpha_{17} RT_{zz} + \alpha_{18} RT_{xx}$$

$$+ \alpha_{19} \frac{RT}{\rho} \rho_{yy} + \alpha_{20} \frac{RT}{\rho} \rho_{zz} + \alpha_{21} \frac{RT}{\rho} \rho_{xx} + \alpha_{22} \frac{RT}{\rho^2} \rho_y^2 + \alpha_{23} \frac{RT}{\rho^2} \rho_z^2 + \alpha_{24} \frac{RT}{\rho^2} \rho_x^2 + \alpha_{25} \frac{R}{T} T_y^2$$

$$+ \alpha_{26} \frac{R}{T} T_z^2 + \alpha_{27} \frac{R}{T} T_x^2 + \alpha_{28} \frac{R}{\rho} T_y \rho_y + \alpha_{29} \frac{R}{\rho} T_z \rho_z + \alpha_{30} \frac{R}{\rho} T_x \rho_x \Big)$$

$$\sigma_{33}^{(2)} = \frac{\mu^2}{p}\Big(\alpha_1 w_z^2 + \alpha_2 w_x^2 + \alpha_3 w_y^2 + \alpha_4 u_z^2 + \alpha_5 u_x^2 + \alpha_{12} v_y w_z + \alpha_{13} w_x u_z + \alpha_{14} u_y v_x + \alpha_{15} v_z w_y$$

$$+\alpha_6 u_y^2+\alpha_7 v_z^2+\alpha_8 v_x^2+\alpha_9 v_y^2+\alpha_{10} w_z u_x+\alpha_{11} u_x v_y+\alpha_{16} RT_{zz}+\alpha_{17} RT_{xx}+\alpha_{18} RT_{yy}$$

$$+\alpha_{19}\frac{RT}{\rho}\rho_{zz}+\alpha_{20}\frac{RT}{\rho}\rho_{xx}+\alpha_{21}\frac{RT}{\rho}\rho_{yy}+\alpha_{22}\frac{RT}{\rho^2}\rho_z^2+\alpha_{23}\frac{RT}{\rho^2}\rho_x^2+\alpha_{24}\frac{RT}{\rho^2}\rho_y^2+\alpha_{25}\frac{R}{T}T_z^2$$

$$+\alpha_{26}\frac{R}{T}T_x^2+\alpha_{27}\frac{R}{T}T_y^2+\alpha_{28}\frac{R}{\rho}T_z\rho_z+\alpha_{29}\frac{R}{\rho}T_x\rho_x+\alpha_{30}\frac{R}{\rho}T_y\rho_y\Big)$$

$$\sigma_{12}^{(2)}=\sigma_{21}^{(2)}=\frac{\mu^2}{p}\Big(\beta_1 u_x u_y+\beta_2 v_x v_y+\beta_3 w_x w_y+\beta_4 u_x v_x+\beta_5 u_y v_y+\beta_6 u_z v_z+\beta_7 u_y w_z$$

$$+\beta_8 v_x w_z+\beta_9 u_z w_y+\beta_{10} v_z w_x+\beta_{11} RT_{xy}+\beta_{12}\frac{RT}{\rho}\rho_{xy}+\beta_{13}\frac{R}{T}T_x T_y+\beta_{14}\frac{RT}{\rho^2}\rho_x\rho_y$$

$$+\beta_{15}\frac{R}{\rho}\rho_x T_y+\beta_{16}\frac{R}{\rho}T_x\rho_y\Big)$$

$$\sigma_{23}^{(2)}=\sigma_{32}^{(2)}=\frac{\mu^2}{p}\Big(\beta_1 v_y v_z+\beta_2 w_y w_z+\beta_3 u_y u_z+\beta_4 v_y w_y+\beta_5 v_z w_z+\beta_6 v_x w_x+\beta_7 v_z u_x$$

$$+\beta_8 w_y u_x+\beta_9 v_x u_z+\beta_{10} w_x u_y+\beta_{11} RT_{yz}+\beta_{12}\frac{RT}{\rho}\rho_{yz}+\beta_{13}\frac{R}{T}T_y T_z+\beta_{14}\frac{RT}{\rho^2}\rho_y\rho_z$$

$$+\beta_{15}\frac{R}{\rho}\rho_y T_z+\beta_{16}\frac{R}{\rho}T_y\rho_z\Big)$$

$$\sigma_{31}^{(2)}=\sigma_{13}^{(2)}=\frac{\mu^2}{p}\Big(\beta_1 w_z w_x+\beta_2 u_z u_x+\beta_3 v_z v_x+\beta_4 w_z u_z+\beta_5 w_x u_x+\beta_6 w_y u_y+\beta_7 w_x v_y$$

$$+\beta_8 u_z v_y+\beta_9 w_y v_x+\beta_{10} u_y v_z+\beta_{11} RT_{zx}+\beta_{12}\frac{RT}{\rho}\rho_{zx}+\beta_{13}\frac{R}{T}T_z T_x+\beta_{14}\frac{RT}{\rho^2}\rho_z\rho_x$$

$$+\beta_{15}\frac{R}{\rho}\rho_z T_x+\beta_{16}\frac{R}{\rho}T_z\rho_x\Bigg)$$

$$q_1^{(2)}=\frac{\mu^2}{\rho}\Bigg(\gamma_1\frac{1}{T}T_x u_x+\gamma_2\frac{1}{T}T_x v_y+\gamma_3\frac{1}{T}T_x w_z+\gamma_4\frac{1}{T}T_y v_x+\gamma_5\frac{1}{T}T_y u_y+\gamma_6\frac{1}{T}T_z w_x+\gamma_7\frac{1}{T}T_z u_z$$

$$+\gamma_8 u_{xx}+\gamma_9 u_{yy}+\gamma_{10}u_{zz}+\gamma_{11}v_{xy}+\gamma_{12}w_{xz}+\gamma_{13}\frac{1}{\rho}\rho_x u_x+\gamma_{14}\frac{1}{\rho}\rho_x v_y+\gamma_{15}\frac{1}{\rho}\rho_x w_z$$

$$+\gamma_{16}\frac{1}{\rho}\rho_y v_x+\gamma_{17}\frac{1}{\rho}\rho_y u_y+\gamma_{18}\frac{1}{\rho}\rho_z w_x+\gamma_{19}\frac{1}{\rho}\rho_z u_z\Bigg)$$

$$q_2^{(2)}=\frac{\mu^2}{\rho}\Bigg(\gamma_1\frac{1}{T}T_y v_y+\gamma_2\frac{1}{T}T_y w_z+\gamma_3\frac{1}{T}T_y u_x+\gamma_4\frac{1}{T}T_z w_y+\gamma_5\frac{1}{T}T_z v_z+\gamma_6\frac{1}{T}T_x u_y+\gamma_7\frac{1}{T}T_x v_x$$

$$+\gamma_8 v_{yy}+\gamma_9 v_{zz}+\gamma_{10}v_{xx}+\gamma_{11}w_{yz}+\gamma_{12}u_{xy}+\gamma_{13}\frac{1}{\rho}\rho_y v_y+\gamma_{14}\frac{1}{\rho}\rho_y w_z+\gamma_{15}\frac{1}{\rho}\rho_y u_x$$

$$+\gamma_{16}\frac{1}{\rho}\rho_z w_y+\gamma_{17}\frac{1}{\rho}\rho_z v_z+\gamma_{18}\frac{1}{\rho}\rho_x u_y+\gamma_{19}\frac{1}{\rho}\rho_x v_x\Bigg)$$

$$q_3^{(2)}=\frac{\mu^2}{\rho}\Bigg(\gamma_1\frac{1}{T}T_z w_z+\gamma_2\frac{1}{T}T_z u_x+\gamma_3\frac{1}{T}T_z v_y+\gamma_4\frac{1}{T}T_x u_z+\gamma_5\frac{1}{T}T_x w_x+\gamma_6\frac{1}{T}T_y v_z+\gamma_7\frac{1}{T}T_y w_y$$

$$+\gamma_8 w_{zz}+\gamma_9 w_{xx}+\gamma_{10}w_{yy}+\gamma_{11}u_{xz}+\gamma_{12}v_{yz}+\gamma_{13}\frac{1}{\rho}\rho_z w_z+\gamma_{14}\frac{1}{\rho}\rho_z u_x+\gamma_{15}\frac{1}{\rho}\rho_z v_y$$

$$+\gamma_{16}\frac{1}{\rho}\rho_x u_z+\gamma_{17}\frac{1}{\rho}\rho_x w_x+\gamma_{18}\frac{1}{\rho}\rho_y v_z+\gamma_{19}\frac{1}{\rho}\rho_y w_y\Bigg)$$

The coefficients $\alpha_i, \beta_i,$ and γ_i in these equations are given in the appendix. The following terms represent the augmented stress and heat flux terms:

$$\sigma_{11}^{(a)} = (\mu^3 / p^2) RT[\alpha_{31} u_{xxx} + \alpha_{32} u_{xyy} + \alpha_{33} u_{xzz} + \alpha_{34} v_{xxy} + \alpha_{35} v_{yyy} + \alpha_{36} v_{yzz} + \alpha_{37} w_{xxz} + \alpha_{38} w_{yyz} + \alpha_{39} w_{zzz}]$$

$$\sigma_{22}^{(a)} = (\mu^3 / p^2) RT[\alpha_{31} v_{yyy} + \alpha_{32} v_{yzz} + \alpha_{33} v_{yxx} + \alpha_{34} w_{yyz} + \alpha_{35} w_{zzz} + \alpha_{36} w_{zxx} + \alpha_{37} u_{yyx} + \alpha_{38} u_{zzx} + \alpha_{39} u_{xxx}]$$

$$\sigma_{33}^{(a)} = (\mu^3 / p^2) RT[\alpha_{31} w_{zzz} + \alpha_{32} w_{zxx} + \alpha_{33} w_{zyy} + \alpha_{34} u_{zzx} + \alpha_{35} u_{xxx} + \alpha_{36} u_{xyy} + \alpha_{37} v_{zzy} + \alpha_{38} v_{xxy} + \alpha_{39} v_{yyy}]$$

$$\sigma_{12}^{(a)} = \sigma_{21}^{(a)} = (\mu^3 / p^2) RT[\beta_{17} u_{yxx} + \beta_{18} u_{yyy} + \beta_{19} u_{yzz} + \beta_{20} v_{xxx} + \beta_{21} v_{xyy} + \beta_{22} v_{xzz}]$$

$$\sigma_{23}^{(a)} = \sigma_{32}^{(a)} = (\mu^3 / p^2) RT[\beta_{17} v_{zxx} + \beta_{18} v_{zyy} + \beta_{19} v_{zzz} + \beta_{20} w_{yxx} + \beta_{21} w_{yyy} + \beta_{22} w_{yzz}]$$

$$\sigma_{31}^{(a)} = \sigma_{13}^{(a)} = (\mu^3 / p^2) RT[\beta_{17} w_{xxx} + \beta_{18} w_{xyy} + \beta_{19} w_{xzz} + \beta_{20} u_{zxx} + \beta_{21} u_{zyy} + \beta_{22} u_{zzz}]$$

$$q_1^{(a)} = (\mu^3 / p\rho) R[\gamma_{20} T_{xxx} + \gamma_{21} T_{xyy} + \gamma_{22} T_{xzz} + \gamma_{23} (T/\rho) \rho_{xxx} + \gamma_{24} (T/\rho) \rho_{xyy} + \gamma_{25} (T/\rho) \rho_{xzz}]$$

$$q_2^{(a)} = (\mu^3 / p\rho) R[\gamma_{20} T_{yxx} + \gamma_{21} T_{yyy} + \gamma_{22} T_{yzz} + \gamma_{23} (T/\rho) \rho_{yxx} + \gamma_{24} (T/\rho) \rho_{yyy} + \gamma_{25} (T/\rho) \rho_{yzz}]$$

$$q_3^{(a)} = (\mu^3 / p\rho) R[\gamma_{20} T_{zxx} + \gamma_{21} T_{zyy} + \gamma_{22} T_{zzz} + \gamma_{23} (T/\rho) \rho_{zxx} + \gamma_{24} (T/\rho) \rho_{zyy} + \gamma_{25} (T/\rho) \rho_{zzz}]$$

The coefficients appearing in these equations are as follows:

$$\alpha_{31} = \alpha_{32} = \alpha_{33} = \omega_7$$

$$\alpha_{34} = \alpha_{35} = \alpha_{36} = \alpha_{37} = \alpha_{38} = \alpha_{39} = -\frac{1}{2}\omega_7$$

$$\beta_{17} = \beta_{18} = \beta_{19} = \beta_{20} = \beta_{21} = \beta_{22} = \frac{3}{4}\omega_7$$

$$\gamma_{20} = \gamma_{21} = \gamma_{22} = \theta_7, \quad \gamma_{23} = \gamma_{24} = \gamma_{25} = \theta_6$$

THE SIMPLIFIED BURNETT EQUATIONS TERMS

The complete BGK equations require too many computer operations to calculate, thereby motivating our interest in a simplified version of the models. For this purpose, we consider a related result from Lumpkin,[13] who proposed the following simplified form:

$$\tau_{ij}^{B} = \varpi \frac{3}{2}\frac{\mu^2}{p}\frac{\partial u_k}{\partial x_k}\left(D_{ij} - 1/3 D_{kk}\delta_{ij}\right),$$

$$q_i^{B} = \vartheta \frac{3}{2}\frac{\mu^2}{\rho T_t}\frac{\partial T_t}{\partial x_i}\frac{\partial u_k}{\partial x_k}.$$

Familiar notations are used in these expressions and

$$D_{ij} = \frac{1}{2}\left(\frac{\partial u^i}{\partial x^j} + \frac{\partial u^j}{\partial x^i}\right).$$

However, ϖ is a stress coefficient and ϑ is a heat flux coefficient. Note that the temperature that appears in the heat flux terms is the translational temperature. In the calculations,

$$\varpi = 8 \text{ and } \theta = \left(\theta_1 + \frac{8}{3}\theta_2 + \frac{2}{3}\theta_3 + \frac{2}{3}\theta_5 \right).$$

The constants in this equation are defined in Table A1.

Other than the investigation in [13], the simplified Burnett equations have not received attention. To learn more about this model, we carried out a linear stability analysis in which the spatial wave number is related to the Knudsen number. To this end, the equations can be written as follows, noting that they contain the translational and Rotational Non-equilibrium terms for a diatomic gas:

$$\frac{\partial \rho}{\partial t} + \frac{\partial (\rho u)}{\partial x} = 0,$$

$$\frac{\partial (\rho u)}{\partial t} + \frac{\partial}{\partial x}\left(p + \rho u^2\right) = -\frac{\partial \tau_{xx}}{\partial x},$$

$$\frac{\partial (\rho E)}{\partial t} + \frac{\partial}{\partial x}\left(pu + \rho E u\right) = -\frac{\partial}{\partial x}\left(u\tau_{xx}\right) - \frac{\partial q}{\partial x},$$

$$\frac{\partial (\rho T_R)}{\partial t} + \frac{\partial}{\partial x}\left(\rho u T_R\right) = \mu \frac{\partial^2 T_R}{\partial x^2} + \frac{4\rho p\left(6T_t - T_R\right)}{5\pi\mu Z_R},$$

$$\tau_{xx} = \left(-\frac{4}{3}\mu + \frac{\pi\mu(\gamma - 1)^2 Z_R}{4} \right)\frac{\partial u}{\partial x} + \frac{8\mu^2}{p}\left(\frac{\partial u}{\partial x}\right)^2,$$

$$q = -\frac{15}{4}\mu R\frac{\partial T_t}{\partial x} + \frac{40}{9}\frac{\mu^2}{\rho T_t}\left(\frac{\partial u}{\partial x}\right)\left(\frac{\partial T_t}{\partial x}\right) - \mu R\frac{\partial T_R}{\partial x},$$

where

$E = \frac{1}{2}\left(3RT_t + 2RT_R + u^2\right)$ = total energy/unit mass,

$p = \rho R T_t$ = hydrodynamic pressure,

T_R = rotational temperature,

T_t = translational temperature,

μ = molecular viscosity,

Z_R = rotational collision number (18 to 23).

Note that τ_R = relaxation time for rotational energy = $Z_R \tau_c = Z_R \left(\frac{\pi \mu}{4p} \right)$ and τ_c = mean collision time.

Linearization of the equations

Consider a diatomic gas in equilibrium with density ρ_0, pressure p_0, translational temperature T_{t0} and rotational temperature T_{R0}. The gas is subjected to small perturbations defined as the non-dimensional variables:

$$\rho' = \frac{\rho - \rho_0}{\rho_0}, \qquad T_t' = \frac{T_t - T_{t0}}{T_{t0}}, \qquad T_R' = \frac{T_R - T_{R0}}{T_{R0}}$$

$$u' = \frac{u}{\sqrt{RT_{t0}}}, \qquad t' = \frac{t}{\mu_0 / \rho_0}, \qquad x' = \frac{x}{L_0}$$

$$L_0 = \frac{\mu_0}{\rho_0 \sqrt{RT_{t0}}}, \qquad \text{Note that } T_{R0} = T_{t0}$$

The linearization results in the following equations in non-dimensional form for small perturbations:

$$\frac{\partial \rho'}{\partial t'} + \frac{\partial u'}{\partial x'} = 0 \tag{9}$$

$$\frac{\partial u'}{\partial t'} + \frac{\partial \rho'}{\partial x'} + \frac{\partial T_t'}{\partial x'} + \left(-\frac{4}{3} + \frac{\pi}{4} (\gamma - 1)^2 Z_R \right) \frac{\partial^2 u'}{\partial x'^2} = 0 \tag{10}$$

$$\frac{\partial T_t'}{\partial t'}+\frac{2}{3}\frac{\partial T_R'}{\partial t'}+\frac{2}{3}\frac{\partial u'}{\partial x'}-\frac{5}{2}\frac{\partial^2 T_t'}{\partial x'^2}-\frac{2}{3}\frac{\partial^2 T_R'}{\partial x'^2}=0 \tag{11}$$

$$\frac{\partial T_R'}{\partial t'}-\frac{\partial^2 T_R'}{\partial x'^2}-\frac{4}{5\pi Z_R}\left[11T_t'-T_R'+10\rho'\right]=\frac{4}{\pi Z_R}$$

Let $C \equiv \frac{4}{5\pi Z_R}$. The last equation becomes

$$\frac{\partial T_R'}{\partial t'}-\frac{\partial^2 T_R'}{\partial x'^2}-C\left[11T_t'-T_R'+10\rho'\right]=5C \tag{12}$$

From equation (12)

$$\frac{\partial T_R'}{\partial t'}=\frac{\partial^2 T_R'}{\partial x'^2}+C\left[11T_t'-T_R'+10\rho'+5\right]$$

Substituting this into equation (11), we obtain

$$\frac{\partial T_t'}{\partial t}+\frac{2}{3}\frac{\partial u'}{\partial x}-\frac{5}{2}\frac{\partial^2 T_t'}{\partial x^2}+\frac{2}{3}C[11T_t'-T_R'+10\rho'+5]=0 \tag{13}$$

We employ equations 9 through 12 in the stability analysis.

Stability Analysis of Linearized Equations

We write the linearized equations as follows:

$$\frac{\partial V'}{\partial t'}+L_1\frac{\partial V'}{\partial x'}+L_2\frac{\partial^2 V'}{\partial x'^2}+L_0V'=A\,, \tag{14}$$

where $V'=\left[\rho' \quad u' \quad T_t' \quad T_R'\right]^T$,

and

$$L_1=\begin{bmatrix}0 & 1 & 0 & 0\\ 1 & 0 & 1 & 0\\ 0 & 2/3 & 0 & 0\\ 0 & 0 & 0 & 0\end{bmatrix}$$

$$L_2 = \begin{bmatrix} 0 & 0 & 0 & 0 \\ 0 & \left\{-\frac{4}{3}+\frac{\pi}{4}(\gamma-1)^2 Z_R\right\} & 0 & 0 \\ 0 & 0 & -5/2 & 0 \\ 0 & 0 & 0 & -1 \end{bmatrix}$$

$$L_0 = C\begin{bmatrix} 0 & 0 & 0 & 0 \\ 0 & 0 & 0 & 0 \\ \frac{20}{3} & 0 & \frac{22}{3} & -\frac{2}{3} \\ -10 & 0 & -11 & 1 \end{bmatrix}$$

$$A = \begin{bmatrix} 0 \\ 0 \\ -\frac{10}{3}C \\ 5C \end{bmatrix}$$

Consider the homogeneous equation (13) for stability:

We assume solutions of the form

$$V' = \overline{V} e^{i\alpha x'} e^{\phi t'}, \tag{14}$$

where

$$\phi = \alpha + i\beta,\ \omega = \frac{2\pi}{L/L_0},\ L_0 = \frac{\mu_0}{\rho_0\sqrt{RT_0}} = 0.783\lambda,\ \omega = 4.92\frac{\lambda}{L} = 4.92K_n.$$

Substituting (15) into (14), we obtain

$$\left[\phi I + i\omega L_1 - \omega^2 L_2 + L_0\right]\cdot\overline{V} = 0.$$

The dispersion relation therefore becomes

$$\det\left|\phi I + i\omega L_1 - \omega^2 L_2 + L_0\right| = 0,$$

or

$$\begin{vmatrix} \phi & i\omega & 0 & 0 \\ i\omega & \phi+\left\{\frac{4}{3}-\frac{\pi}{4}(\gamma-1)Z_R\right\}\omega^2 & i\omega & 0 \\ \frac{20}{3}C & i\frac{2}{3}\omega & \phi+\frac{5}{2}\omega^2+\frac{22}{3}C & -\frac{2}{3}C \\ -10C & 0 & -11C & \phi+\omega^2+C \end{vmatrix}=0.$$

This can be simplified to

$$\phi\begin{vmatrix} \phi+\left[\frac{4}{3}-\frac{\pi}{4}(\gamma-1)Z_R\right]\omega^2 & i\omega & 0 \\ i\frac{2}{3}\omega & \phi+\frac{5}{2}\omega^2+\frac{22}{3}C & -\frac{2}{3}C \\ 0 & -11C & \phi+\omega^2+C \end{vmatrix}$$

$$-i\omega\begin{vmatrix} i\omega & i\omega & 0 \\ \frac{20C}{3} & \phi+\frac{5}{2}\omega^2+\frac{22}{3}C & -\frac{2}{3}C \\ -10C & -11C & \phi+\omega^2+C \end{vmatrix}=0,$$

$$\left\{\phi\left[\phi+\left\{\frac{4}{3}-\frac{\pi}{4}(\gamma-1)Z_R\right\}\omega^2\right]\left[\left(\phi+\frac{5}{2}\omega^2+\frac{22}{3}C\right)\left(\phi+\omega^2+C\right)-\frac{22}{3}C^2\right]\right.$$

$$-\phi i^2\omega^2\frac{2}{3}\left(\phi+\omega^2+C\right)-i^2\omega^2\left[\left(\varphi+\frac{5}{2}\omega^2+\frac{22}{3}C\right)\left(\phi+\omega^2+C\right)-\frac{22}{3}C^2\right]$$

$$\left.+i^2\omega^2\left[\left(\phi+\omega^2+C\right)\frac{20}{3}C-\frac{20}{3}C^2\right]\right\}=0,$$

or

$$\left[\left(\phi+\frac{5}{2}\omega^2+\frac{22}{3}C\right)\left(\phi+\omega^2+C\right)-\frac{22}{3}C^2\right]\left[\phi^2+\left(\frac{4}{3}-\frac{\pi}{4}(\gamma-1)Z_R\right)\omega^2\phi+\omega^2\right]$$

$$+\omega^2\left[\frac{2}{3}\phi\left(\phi+\omega^2+C\right)-\left(\phi+\omega^2+C\right)\frac{20}{3}C+\frac{20}{3}C^2\right]=0.$$

The final form of the equation was solved using MATLAB in order to determine the stability boundaries for Z_R = 4, 10, 18, and 23. Note that in Bird's text, a value of approximately 5 is used, although Lumpkin recommended $18 \le Z_R \le 23$ for his simplified model. Also note that Jean's equation [19] has been used in the foregoing, in order to obtain the source term.

The stability boundaries are shown in Figures 1 through 4 below for the various values of Z_R. Regions with negative values of α (on the *x*-axis) are stable, whereas regions with $\alpha > 0$ are unstable. The main parameter is Z_R and Gamma=1.4 for a diatomic gas. Note that $\phi = \alpha + i\beta$, so that α must be negative for stability.

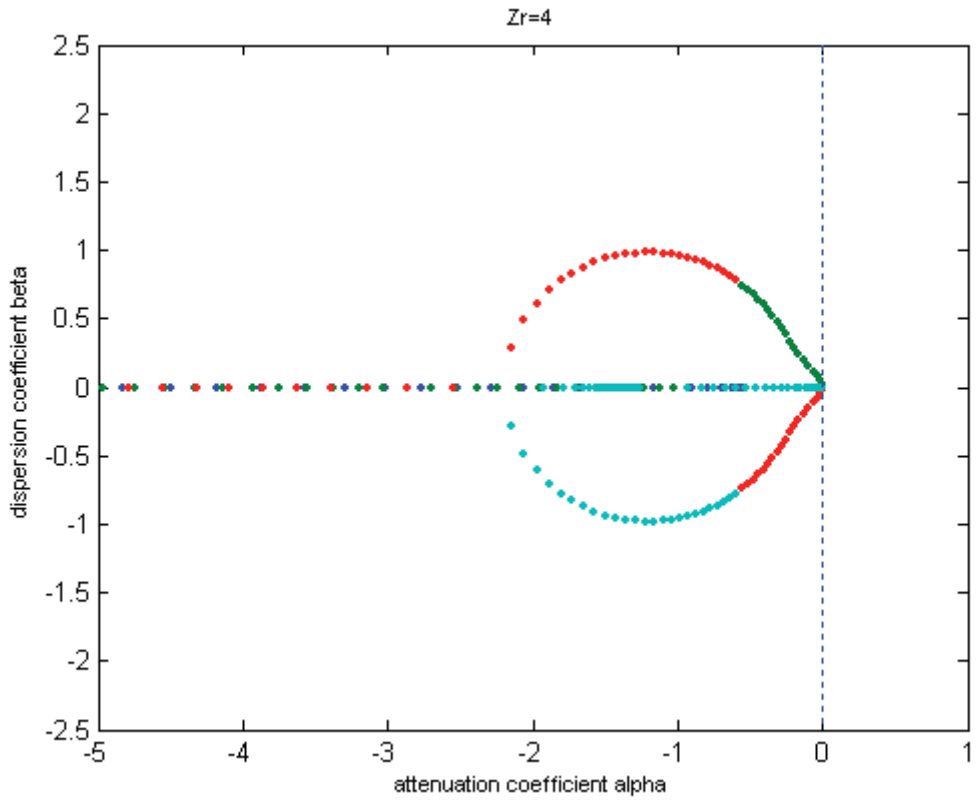

Figure 1: Stability boundaries of Lumpkin's simplified Burnett model for Z_R=4

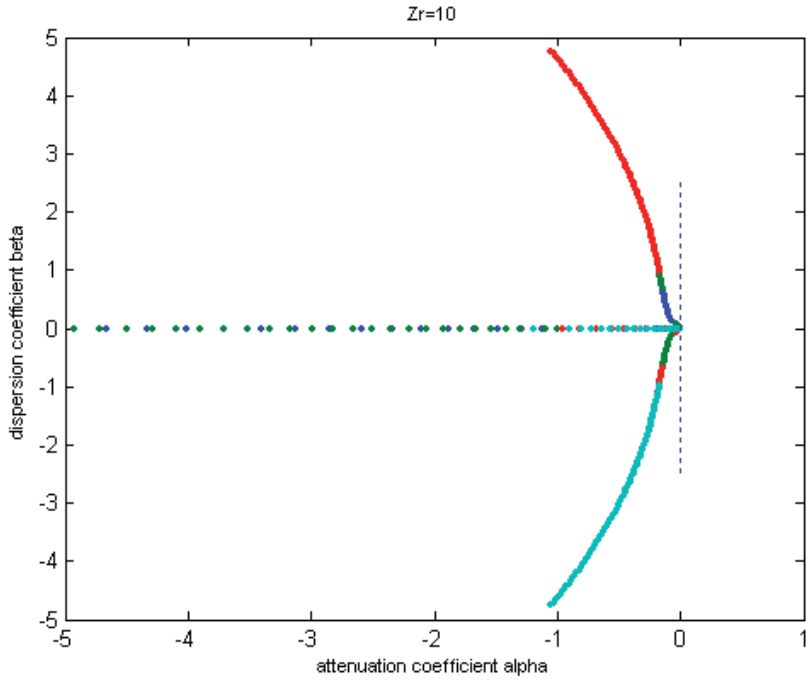

Figure 2: Stability boundaries of Lumpkin's simplified Burnett model for Z_R=10

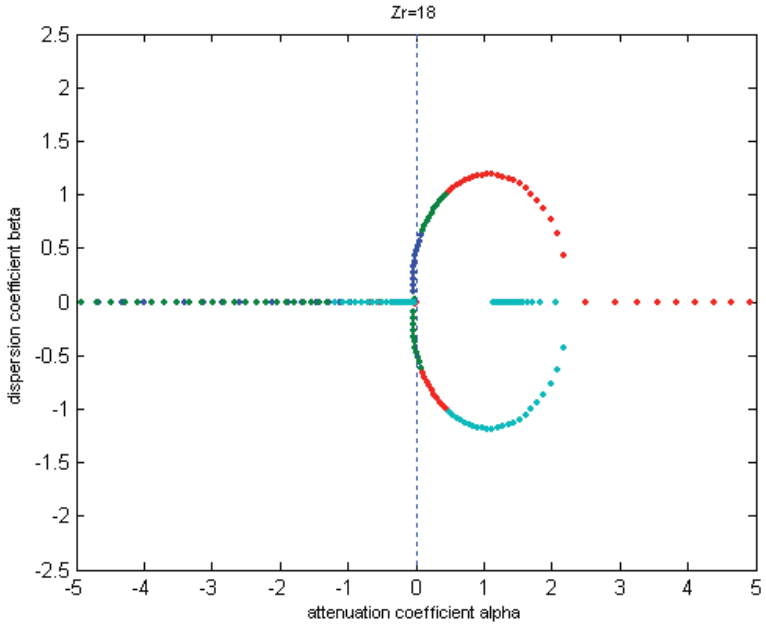

Figure 3: Stability boundaries of Lumpkin's simplified Burnett model for Z_R=18

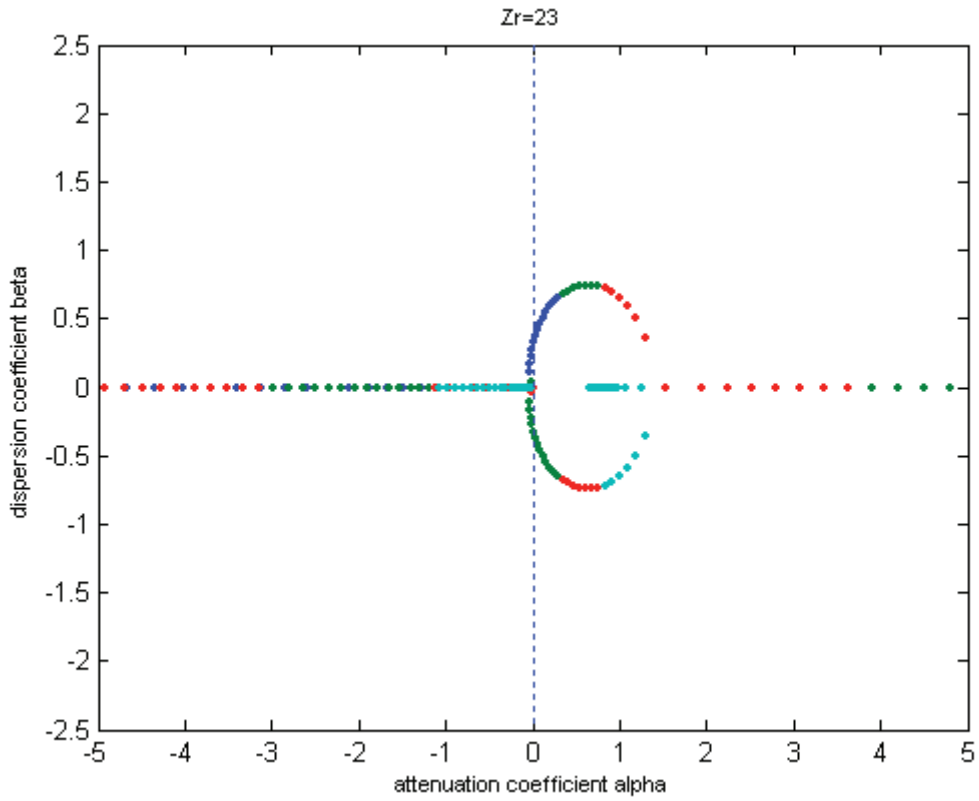

Figure 4: Stability boundaries of Lumpkin's simplified Burnett model for Z_R=23

It is appararent that the equations are unstable to small perturbations in a quiescent fluid when Z_R> 10 and stable otherwise. Thus, although the simplified model seems to work well in some cases, it will be necessary use either the Augmented or BGK-Burnett model to include the rotational non-equilibrium. Note that $\omega = 4.92K_n$, and that the stability boundaries have been determined by varying the K_n from 0 to 1 using 100 points. We have also examined the stability of a one-dimensional Augmented Burnett equations for Z_R=4,18, and 23 (not shown) and found it to be stable for Z_R> 23, with the appropriate choice of coefficients. This suggests the superiority of the augmented Burnett equations over Lumpkin's simplified model.

HOC Calculations

In this section, we report on the calculation of Alsmeyer [15] hypersonic shock tube measurements and flow over a sphere. For the shock tube problem, we compare results obtained with the HOC methods with measurements and the DSMC results. The DSMC code used for the present demonstration was developed in-house. Results are presented for Argon and Nitrogen (N_2). For the sphere, we compare HOC results with those from Navier-Stokes (NS) and DSMC. Note that the base NS code in the HOC procedure is LAURA [16], to which we have added the Burnett terms during the course of the present investigation.

The initial conditions for the shock tube problem are as follows: $T_1 = 300K, \rho_1 = 3.51\times10^{-6}, p_1 = 1/\gamma M_1^2$, where various values of M_1 in the range $1.55 \le M_1 \le 11$ are specified. $\gamma = (1.4, 1.667)$ for N_2 and Ar, respectively. The initial values $T_2, \rho_2, p_2,$ and M_2 at the other end of the shock wave were obtained with the Rankine-Hugoniot relations. For the perfect gas calculations, Sutherland law is used for the dynamic viscosity: $\frac{\mu}{\mu_0} = \left(\frac{T}{T_0}\right)^{3/2} \frac{T_0 + S}{T + S}$, where $S = (1.4, 107, 111)$ for argon, nitrogen, and air, respectively, and $T_0 = 273$ K. Prandtl number, Pr, is 0.71, and thermal conductivity $k = C_p \mu / \Pr$, where C_p is the specific heat at constant pressure. The thermodynamic property calculation procedures described in [16] are used to obtain the values of these quantities for the nonequilibrium calculations. For boundary conditions, we specify the values of the variables at the inflow to the shock wave and zero-gradient at the other boundaries. The translational and (mean) vibrational temperatures are computed. The domain runs from -10 to 10, after being normalized by the mean free path, $\lambda = (0.0175, 0.02566)$ for N_2 and Ar, respectively. The following table summarizes the conditions used for the DSMC calculations for $M_1 = 11$ (Ar) and $M_1 = 10$ (N_2).

Table I Parameters for the DSMC calculations

Parameter	Ar	N_2
Number of particles at end of simulation	20,000	18,440
Number cells, N	300	300
Upstream λ or λ_1	1.47195×10^{-2}	1.31746×10^{-2}
Number density, n	1.0×10^{20}	1.0×10^{20}
Upstream density, ρ_1	6.63×10^{-6}	4.65×10^{-6}
Upstream temperature, T_1	$293K$	$293K$
Z_R	N/A (monoatomic)	5
μ	$\mu_{ref}\left(T/T_{ref}\right)^{\omega}$	$\mu_{ref}\left(T/T_{ref}\right)^{\omega}$
μ_{ref}	2.117×10^{-5}	1.656×10^{-5}
T_{ref}	$273K$	$273K$
ω	.72	.72
Molecular model	VSS, $\alpha=1.4$	VHS
Total number of time steps	800,000	800,000
Time step for first sampling	8,000	8,000
Frequency of sampling	4	4
Total number of samples	2×10^5	2×10^5
Δt	0.75×10^{-6}	0.75×10^{-6}

For the hypersonic flow over a sphere, we tested the cases:

$U_\infty = 2500 m/s, T_\infty = 300K, \rho_\infty = 3.51\times10^{-6} kg/m^3$,

$U_\infty = 5000, T_\infty = 300K, \rho_\infty = 3.51\times10^{-6} kg/m^3$,

$U_\infty = 2500, T_\infty = 200K, \rho_\infty = 0.001$, and $U_\infty = 5000, T_\infty = 200K, \rho_\infty = 0.001$.

(Pr=0.71 in all cases.) Unit of density is kg/m^3, while velocity is in m/s. The upstream conditions are used as the initial conditions for the HOC calculations. For DSMC, a zero initial value for every variable is used. This is essentially a steady calculation via time-stepping. A total of 1500 time steps were required to drive the residual smaller than 1×10^{-5}. Zero-gradient conditions are applied at the outflow. Symmetry conditions are used to solve half of the domain in HOC. The whole domain is analyzed for the DSMC calculations, using a grid of $100\times100\times100$.

RESULTS, DISCUSSIONS, AND CONCLUSIONS

The shock tube calculations are shown in Figures 5 through 11 while the hypersonic sphere calculations are shown in Figures 12 through 23. Note that the emphasis in the results is placed on the performance of the Burnett equations. That is, in relation to the experiments or the DSMC calculations, which are used as the "standard." It is apparent in Figure 5 that the simplified Burnett models show considerable improvement over the Navier-Stokes calculations for both perfect gas (PG) and non-equilibrium (NE) calculations. We also see in this figure that the non-equilibrium results are more accurate (than the perfect gas results). Figure 6 shows that the results from our DSMC procedure compare very well with those from the experiments of Alsmeyer. The experimental results in Figure 7 are intermediate between the results from the simplified Burnett models and the DSMC solutions, showing that some differences do indeed exist between the DSMC results and Alsmeyer's measurements for nitrogen. However, the results from the two methods are close - both are able to predict the overshoot in the translational temperature, when compared with the simplified Burnett results. The calculation of the translational temperature by the Burnett model is unsatisfactory. Note that in Figure 7, the density results agree more than the translational temperature results do, supporting the suggestion of the inadequacy of the non-equilibrium temperature models used.

Figure 8 shows superior performance of the Burnett models relative to the Navier-Stokes calculations, particularly at the higher Mach numbers. Comparison of Figure 7 (N_2) and Figure 9 (Ar) clearly shows superior performance (for translational energy) of the simplified Burnett equations for Ar relative to N_2. This is probably due to the neglect of the rotational temperature in the present HOC calculations. Being diatomic, rotational energy must be included in the calculations for nitrogen (Lumpkin [13]). Fairly good results for the reciprocal thickness by the simplified Burnett equations can also be observed (Figure 11).

Concerning the hypersonic flow over a sphere, we see in Figures 12 through 15 that the Burnett equations give superior results compared to the the Navier-Stokes model (thicker layers) for the various cases. In Figure 16, the need for the inclusion of better temperature models, e.g. the addition of rotational or multi-species vibrational models, is indicated, although the Burnett results are significantly superior to the Navier-Stokes results. Figure 19 shows the profiles of the translational temperature and the mean vibrational temperature, confirming that the non-equilibrium temperature situation exists in this problem. Figure 21 shows evidence of non-equilibrium chemistry, which must be allowed in order to correctly calculate the hypersonic sphere problem. Note that the mass fractions of the nitrogen molecule are dominant relative to those of the nitrogen atom. However, the latter quantities are significant. Figure 20 (U_∞=5000 m/s) shows very large values of density compared to the results in Figure 18 (U_∞=2500 m/s), a direct consequence of the extent of compressibility (Mach number). The discrepancy between

the Navier-Stokes and Burnett results is shown in Figure 17. From Figure 22, we see that non-equilibrium effects are negligible close to the wall, when U_∞ = 5000 m/s, whereas they are apparent when $0.05 \le x \le 0.1$.

In conclusion, we have developed and tested a unified numerical methodology for calculating flows involving the continuum and rarefied regimes, as well as the transitional regime. The superiority of a simplified Burnett model over the Navier-Stokes model has been demonstrated with the Alsmeyer's shock tube problem and hypersonic flow over a sphere. The calculations were carried out in a model environment that includes both thermal and chemical non-equilibrium. The Burnett models constitute a component of our proposed hybrid scheme, which models the purely continuum regime and high order corrections to this regime in the non-equilibrium realm. We have also shown the performance of our DSMC solver, which constitutes the other component of the hybrid scheme. Note that the addition of rotational temperature is necessary to model the hypersonic flow of diatomic gases. Although the results presented in this paper neglected these effects, these capabilities are contained in our HOC model.

Acknowledgements

The work reported in this paper is supported by the United States Air Force Research Laboratory. We appreciate the support provided by Dr. Peter Gnoffo of NASA Langley Research Center. Peter developed the original LAURA code.

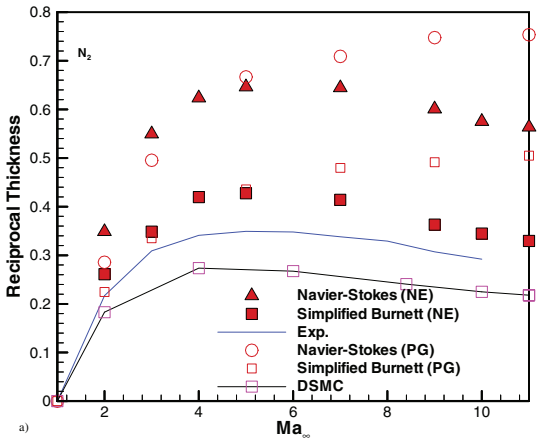

Figure 5: Shock wave reciprocal thickness for nitrogen

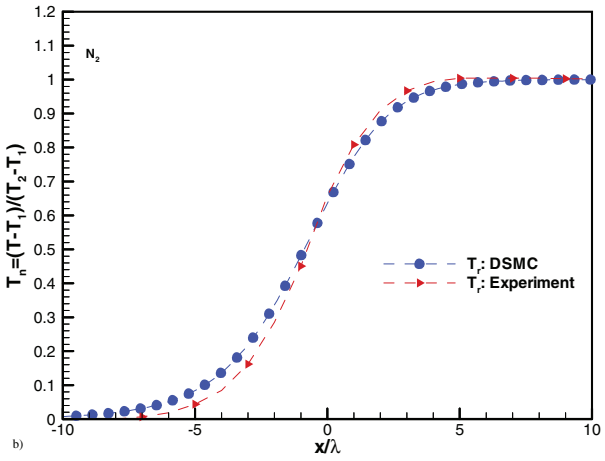

Figure 6: Mach 10 temperature profiles for nitrogen

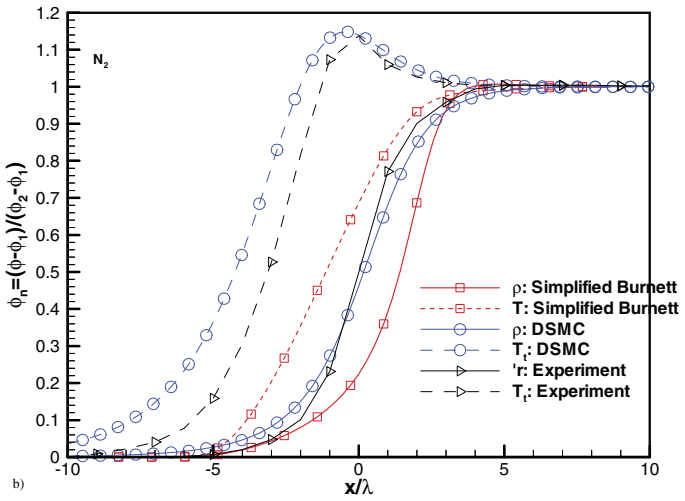

Figure 7: Density and temperature for nitrogen at Mach 10

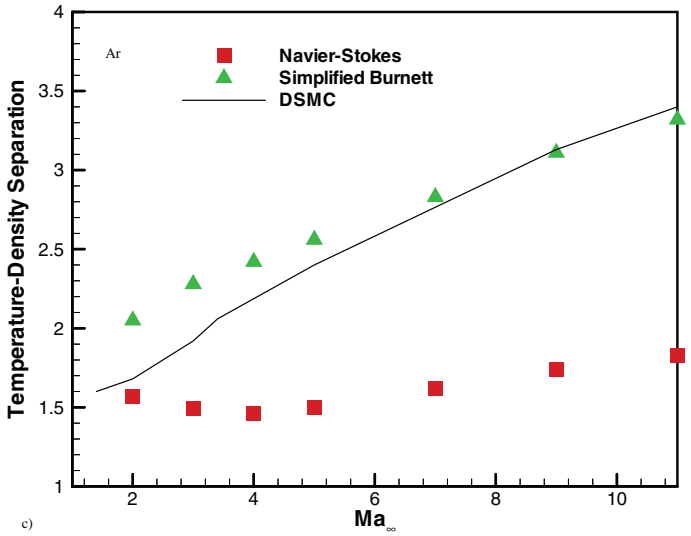

Figure 8: Temperature-density separation for argon

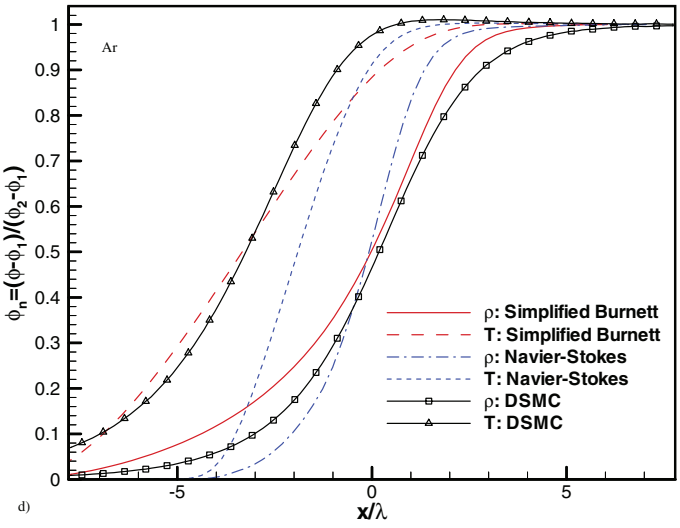

Figure 9: Temperature and density profile for argon at Mach 11

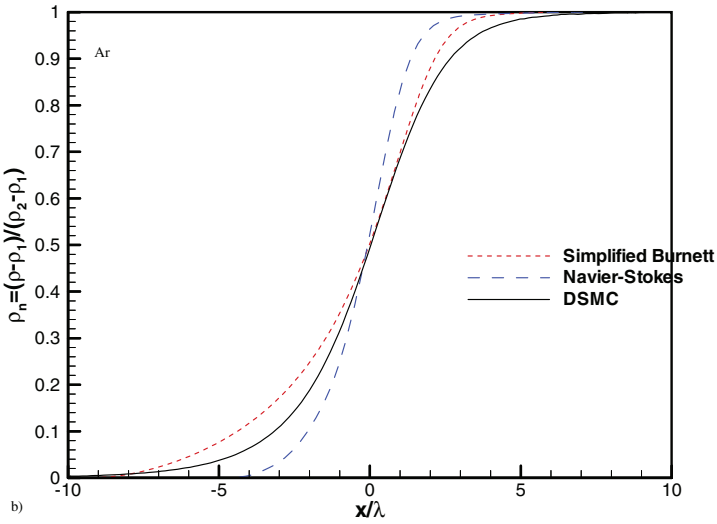

Figure 10: Density profile for argon at Mach 11

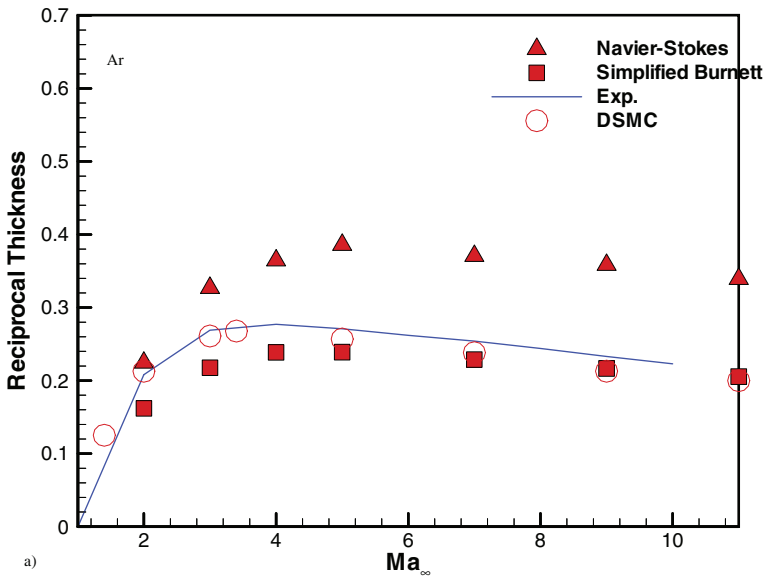

Figure 11: Shock wave reciprocal thickness for argon at Mach 11

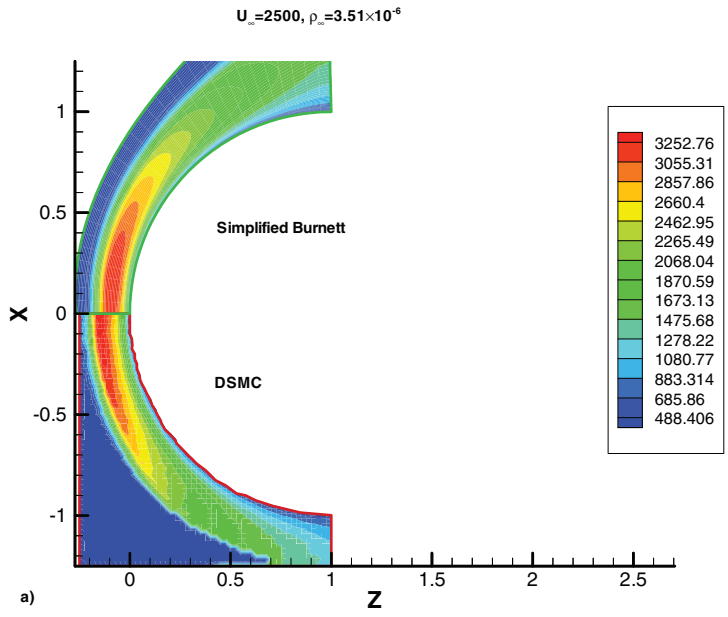

Figure 12: Translational temperature for hypersonic flow over a sphere

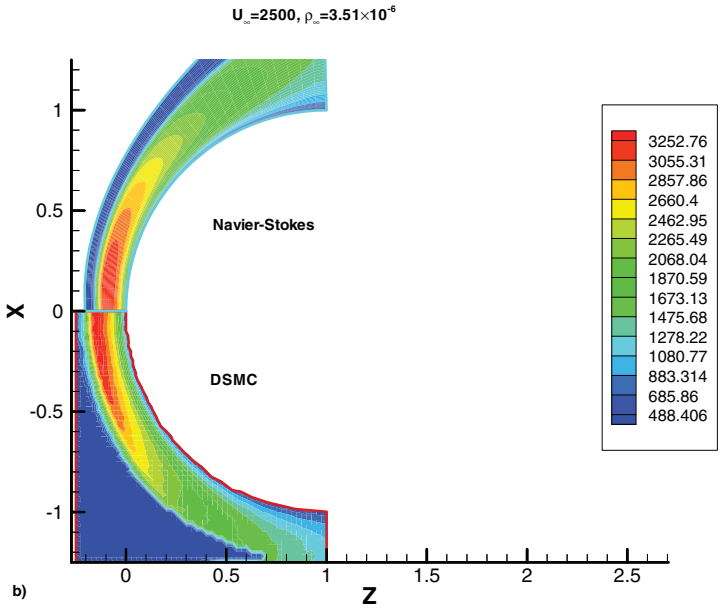

Figure 13: Translational temperature for hypersonic flow over a sphere

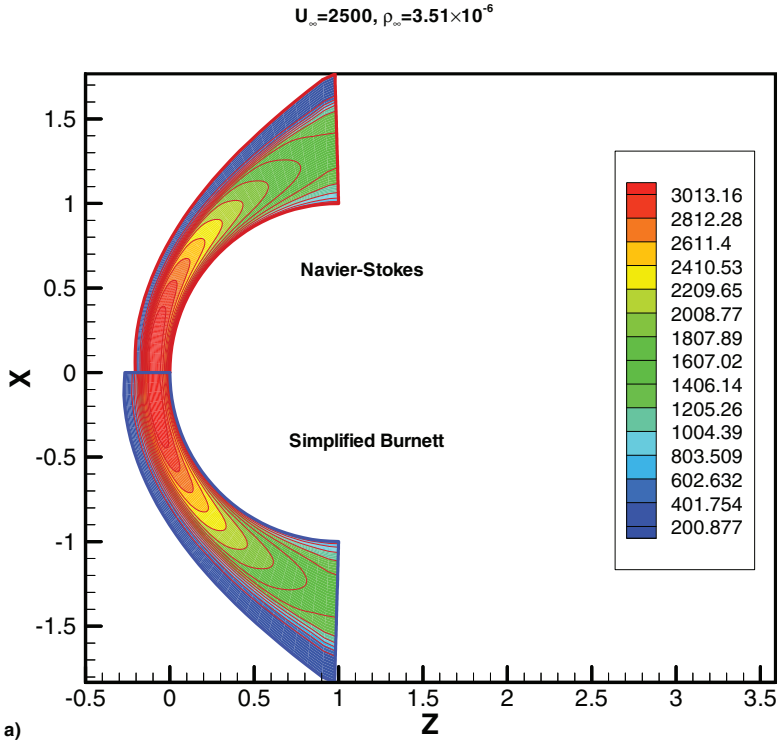

Figure 14: Translational temperature for hypersonic flow over a sphere

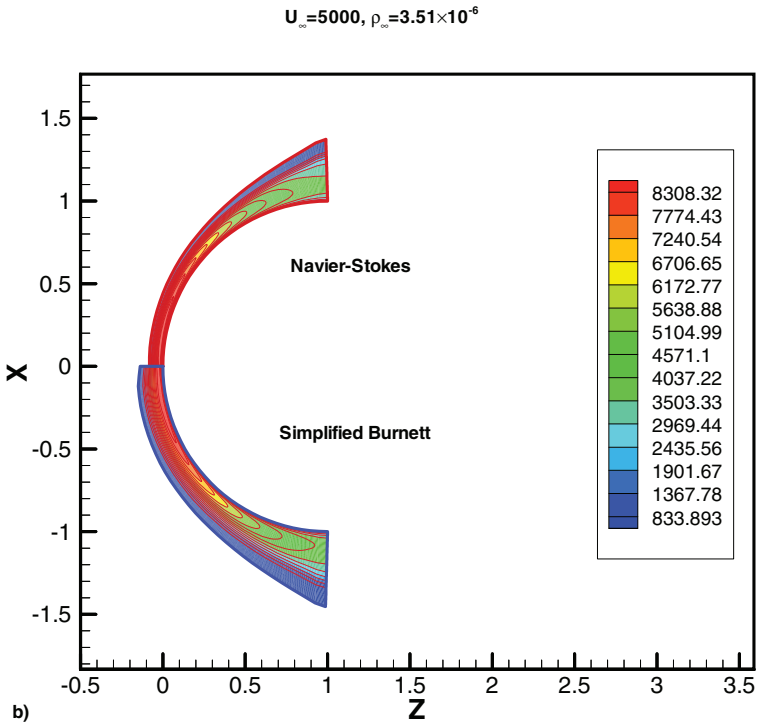

Figure 15: Translational temperature for hypersonic flow over a sphere

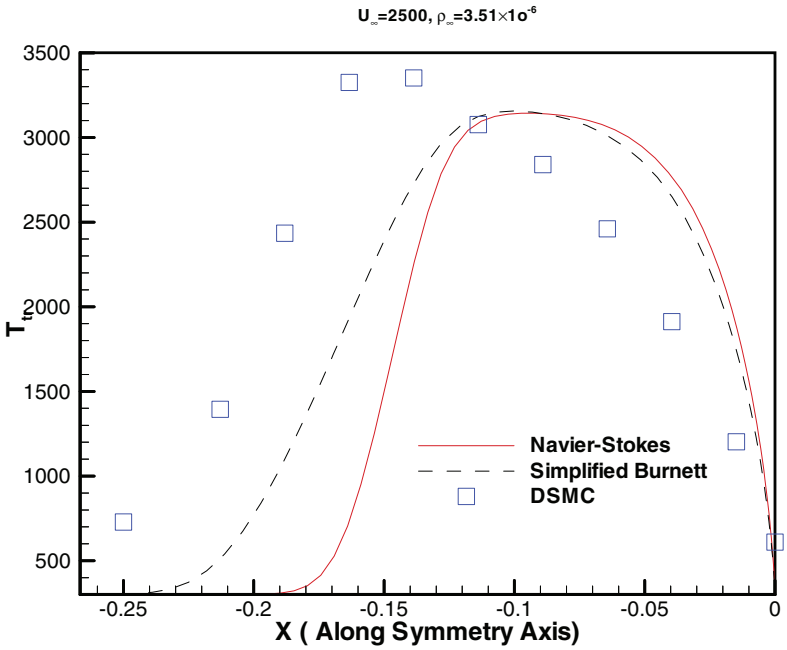

Figure 16: Translational temperature over the surface of the sphere

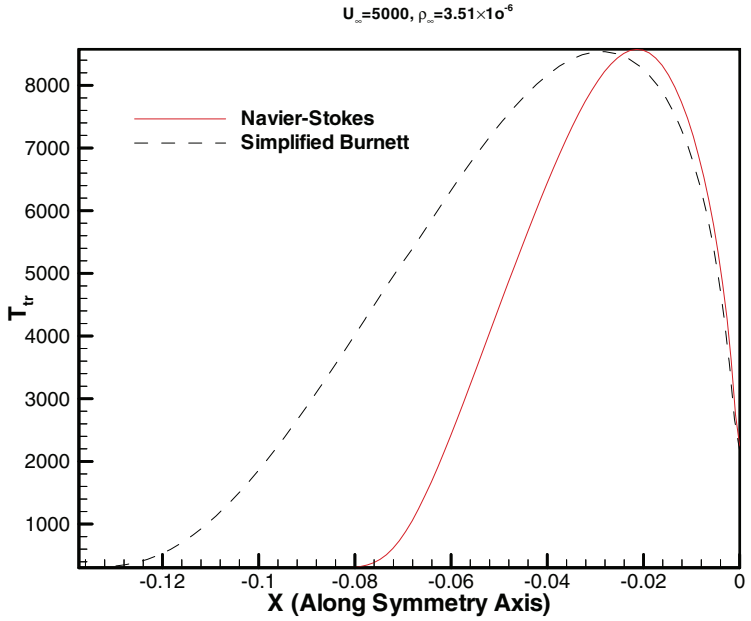

Figure 17: Translational temperature over the surface of the sphere

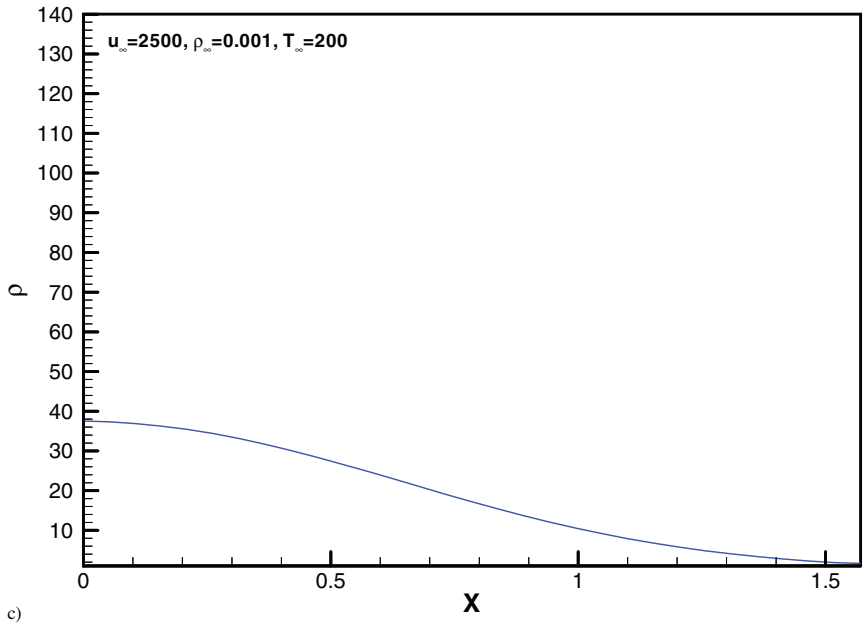

c)

Figure 18: Density profile over the surface of the sphere

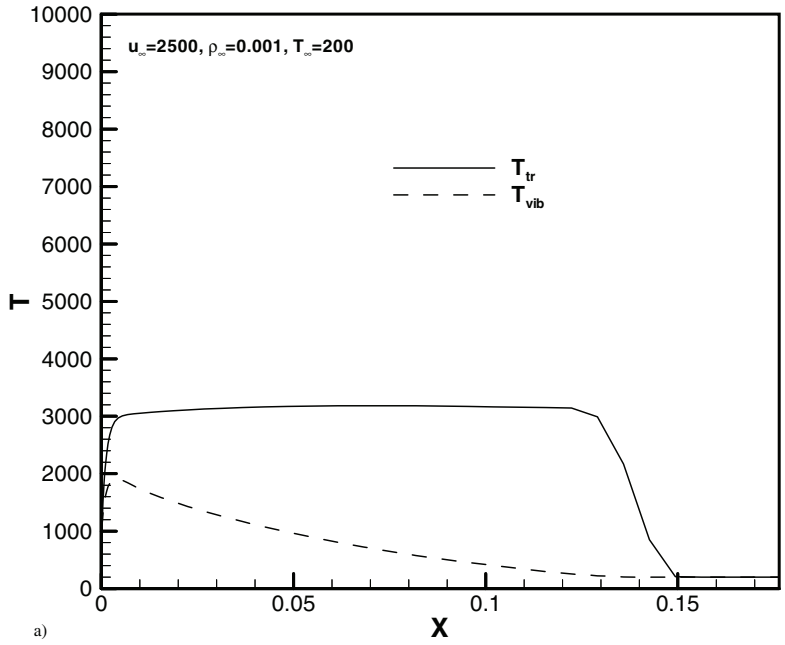

Figure 19: Translational and rotational temperatures along the symmetry axis in front of the sphere

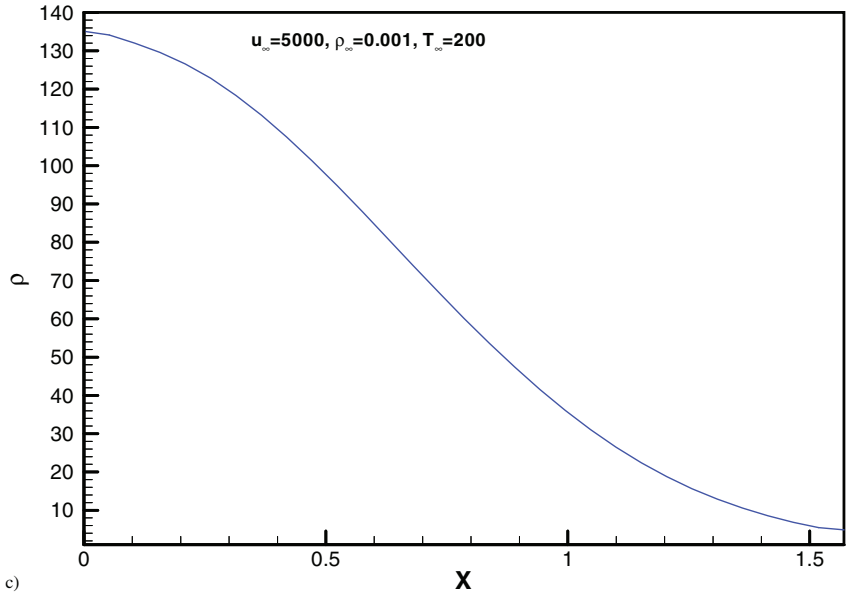

Figure 20: Density profile over the surface of the sphere

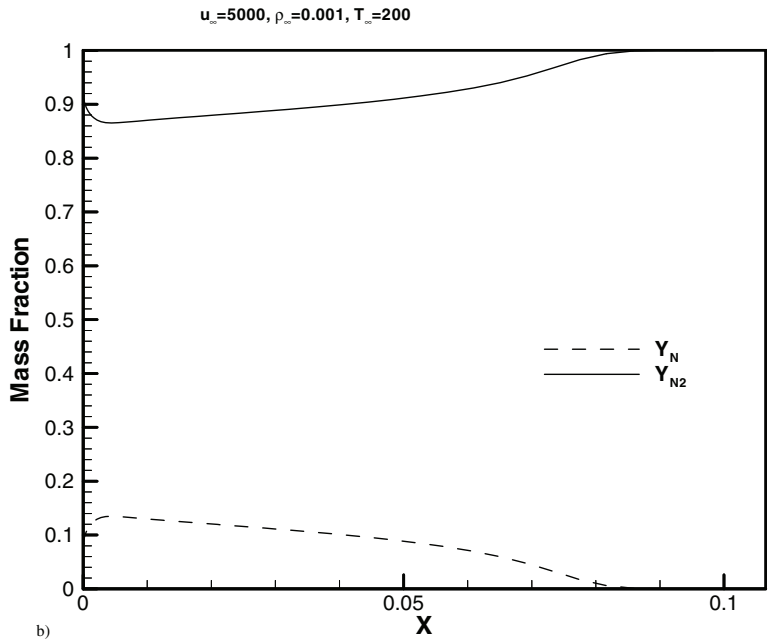

Figure 21: Mass fraction of nitrogen atom and molecule along the symmetry axis in front of the sphere

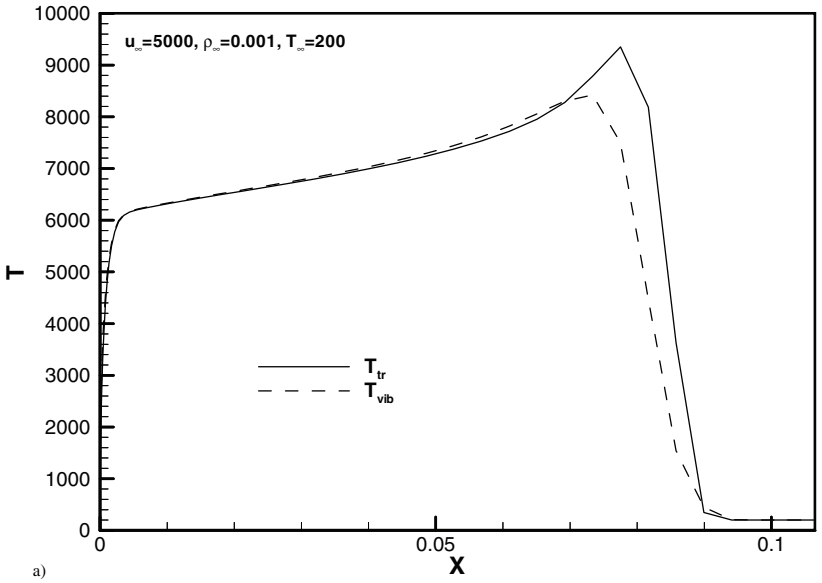

Figure 22: Translational and vibrational temperature along the symmetry axis in front of the sphere

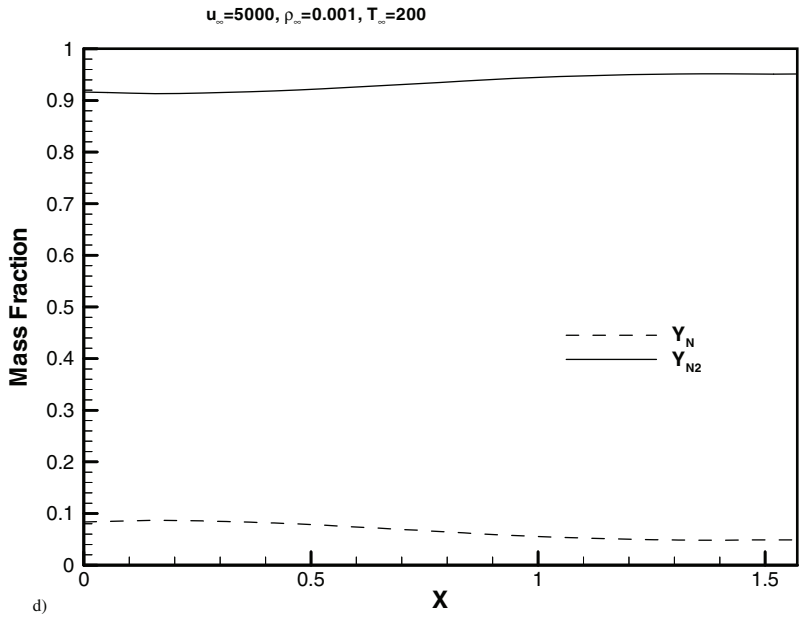

Figure 23: Mass fraction of nitrogen atom and molecule over the surface of the sphere

References

[1] G. A. Bird, Molecular Gas Dynamics and Direct Simulation of Gas Flows, first ed., Oxford University Press, 1994.

[2] E. S. Oran, C. K. Oh, B. Z. Cybyk, Direct Simulation Monte Carlo: Recent Advances and Applications, Annual Review of Fluid Mechanics, 30 (1998), 403-441.

[3] M.S. Ivanov, S. F. Gimelshein, Computational Hypersonic Rarefied Flows, Annual Review of Fluid Mechanics, 30 (1998), 469-505.

[4] W. Li, F. Ladeinde, Analysis of Underexpanded Rarefied Jets, AIAA Journal, Vol. 49, No. 11, (2011), pp. 2581-2585.

[5] R. K. Agarwal, R. Balakrishnan, K. –Y. Yun, Beyond Navier-Stokes: Burnett Equations for Simulation of Hypersonic Flows in Continuum-Transition Regime, in: Dietrich Stauffer (Ed.), Annual Review of Computational Physics, Vol. IX, World Scientific Press, 2001, pp. 211-252.

[6] K.-Y. Yun, R. K. Agarwal, Numerical Simulation of Three-Dimensional Augmented Burnett Equations for Hypersonic Flow, Journal of Spacecraft and Rockets, 38 (2001), 520-533.

[7] B. C. Eu, Kinetic Theory and Irreversible Thermodynamics, first ed., John Wiley & Sons, New York, 1992.

[8] H. Grad, On the Kinetic Theory of Rarefied Gases, Commun. Pure Appl. Math., 2 (1949), 325-331.

[9] V. V. Aristov, F. G. Tcheremissin, The Kinetic Numerical Method for Rarefied and Continuum Gas Flows, in: Rarefied Gas Dynamics, Vol. 1, Plenum Press, New York, 1985, 269-276.

[10] J. Eggers, A. E. Beylich, Development of a hybrid scheme and its application to a flat plate flow, in: J. Harvey, G. Lord (Eds.), Proceedings of the 19th International Symposium on Rarefied Gas Dynamics, vol. 2, Oxford University Press, Oxford, 1995, pp. 1216–1222.

[11] A. L. Garcia, J. B. Bell, W. Y. Crutchfield, B. J. Alder, Adaptive Mesh and Algorithm Refinement Using Direct Simulation Monte Carlo, J. of Computational Physics, 154 (1999), 134-155.

[12] I. D. Boyd, Predicting breakdown of the continuum equations under rarefied flow conditions, in: Rarefied Gas Dynamics, 23rd International Symposium, 2002, Whistler, British Columbia, Canada, pp. 899-906.
[13] F. E. Lumpkin, Development and evaluation of continuum models for translational-rotational non-equilibrium. Ph.D. Thesis, 1990, Department of Aeronautics and Astronautics, Stanford University, Palo Alto, California, USA
[14] K. A. Fiscko, Study of continuum higher order closure models evaluated by a statistical theory of shock structure. Ph.D. Thesis, 1988, Department of Aeronautics and Astronautics, Stanford University, Palo Alto, California, USA
[15] H. Alsmeyer, Density profiles in argon and nitrogen shock waves measured by the absorption of an electron beam, Journal of Fluid Mechanics 74 (1976), 497-513.
[16] P. A. Gnoffo, R. N. Gupta, J. L. Shinn, Conservation equations and physical models for hypersonic air flows in thermal and chemical nonequilibrium", 1989, NASA Technical Paper 2867.
[17] E. Josyula, W. F. Bailey, Governing equations for weakly ionized plasma flow fields of aerospace vehicles,'' AIAA Paper 2002-2228, 33rd AIAA Plasmadynamics and Lasers Conference, May 20-23, 2002, Maui, HI.
[18] J.-H. Lee, Basic governing equations for the flight regimes of aeroassisted orbital transfer vehicles, 96 of Progress in Aeronautics and Astronautics, 96 (1985) AIAA, Inc. (Publisher), pp. 3-53.
[19] J. H. Jeans, On the theory of star-streaming and the structure of the universe, Monthly Notices of the Royal Astronomical Society, 76 (1915), pp. 70-84.

APPENDIX: COEFFICIENTS OF THE BURNETT-ORDER STRESS AND HEAT FLUX TERMS

The coefficients of the Burnett-order (second order) stress and heat flux terms are as follows:

$$\alpha_1 = \frac{2}{3}\omega_1 - \frac{14}{9}\omega_2 + \frac{2}{9}\omega_6, \qquad \alpha_2 = \frac{1}{3}\omega_2 + \frac{1}{12}\omega_6$$

$$\alpha_3 = \frac{1}{3}\omega_2 + \frac{1}{12}\omega_6, \qquad \alpha_4 = -\frac{2}{3}\omega_2 + \frac{1}{12}\omega_6$$

$$\alpha_5 = -\frac{1}{3}\omega_1 + \frac{7}{9}\omega_2 - \frac{1}{9}\omega_6, \qquad \alpha_6 = \frac{1}{3}\omega_2 - \frac{1}{6}\omega_6$$

$$\alpha_7 = -\frac{2}{3}\omega_2 + \frac{1}{12}\omega_6, \qquad \alpha_8 = \frac{1}{3}\omega_2 - \frac{1}{6}\omega_6$$

$$\alpha_9 = -\frac{1}{3}\omega_1 + \frac{7}{9}\omega_2 - \frac{1}{9}\omega_6 \qquad \alpha_{10} = \frac{1}{3}\omega_1 + \frac{2}{9}\omega_2 - \frac{2}{9}\omega_6$$

$$\alpha_{11} = -\frac{2}{3}\omega_1 - \frac{4}{9}\omega_2 + \frac{4}{9}\omega_6 \qquad \alpha_{12} = \frac{1}{3}\omega_1 + \frac{2}{9}\omega_2 - \frac{2}{9}\omega_6$$

$$\alpha_{13} = -\frac{2}{3}\omega_2 + \frac{1}{6}\omega_6 \qquad \alpha_{14} = \frac{4}{3}\omega_2 - \frac{1}{3}\omega_6$$

$$\alpha_{15} = -\frac{2}{3}\omega_2 + \frac{1}{6}\omega_6 \qquad \alpha_{16} = -\frac{2}{3}\omega_2 + \frac{2}{3}\omega_3$$

$$\alpha_{17} = \frac{1}{3}\omega_2 - \frac{1}{3}\omega_3 \qquad \alpha_{18} = \frac{1}{3}\omega_2 - \frac{1}{3}\omega_3$$

$$\alpha_{19} = -\frac{2}{3}\omega_2 \qquad \alpha_{20} = \frac{1}{3}\omega_2$$

$$\alpha_{21} = \frac{1}{3}\omega_2 \qquad \alpha_{22} = \frac{2}{3}\omega_2$$

$$\alpha_{23} = -\frac{1}{3}\omega_2 \qquad \alpha_{24} = -\frac{1}{3}\omega_2$$

$$\alpha_{25} = \frac{2}{3}\omega_4 + \frac{2}{3}\omega_5 \qquad \alpha_{26} = -\frac{1}{3}\omega_4 - \frac{1}{3}\omega_5$$

$$\alpha_{27} = -\frac{1}{3}\omega_4 - \frac{1}{3}\omega_5 \qquad \alpha_{28} = -\frac{2}{3}\omega_2 + \frac{2}{3}\omega_4$$

$$\alpha_{29} = \frac{1}{3}\omega_2 - \frac{1}{3}\omega_4 \qquad \alpha_{30} = \frac{1}{3}\omega_2 - \frac{1}{3}\omega_4$$

$$\beta_1 = \frac{1}{2}\omega_1 - \frac{5}{3}\omega_2 + \frac{1}{6}\omega_6 \qquad \beta_2 = \frac{1}{2}\omega_1 - \frac{5}{3}\omega_2 + \frac{1}{6}\omega_6$$

$$\beta_3 = -\omega_2 + \frac{1}{4}\omega_6 \qquad \beta_4 = \frac{1}{2}\omega_1 - \frac{2}{3}\omega_2 + \frac{1}{6}\omega_6$$

$$\beta_5 = \frac{1}{2}\omega_1 - \frac{2}{3}\omega_2 + \frac{1}{6}\omega_6 \qquad \beta_6 = \frac{1}{4}\omega_6$$

$$\beta_7 = \frac{1}{2}\omega_1 + \frac{1}{3}\omega_2 - \frac{1}{3}\omega_6 \qquad \beta_8 = \frac{1}{2}\omega_1 + \frac{1}{3}\omega_2 - \frac{1}{3}\omega_6$$

$$\beta_9 = -\omega_2 + \frac{1}{4}\omega_6 \qquad \beta_{10} = -\omega_2 + \frac{1}{4}\omega_6$$

$$\beta_{11} = -\omega_2 + \omega_3 \qquad \beta_{12} = -\omega_2$$

$$\beta_{13} = \omega_4 + \omega_5 \qquad \beta_{14} = \omega_2$$

$$\beta_{15} = -\frac{1}{2}\omega_2 + \frac{1}{2}\omega_4 \qquad \beta_{16} = -\frac{1}{2}\omega_2 + \frac{1}{2}\omega_4$$

$$\gamma_1 = \theta_1 + \frac{8}{3}\theta_2 + \frac{2}{3}\theta_3 + \frac{2}{3}\theta_5 \qquad \gamma_2 = \theta_1 + \frac{2}{3}\theta_2 - \frac{1}{3}\theta_3 - \frac{1}{3}\theta_5$$

$$\gamma_3 = \theta_1 + \frac{2}{3}\theta_2 - \frac{1}{3}\theta_3 - \frac{1}{3}\theta_5 \qquad \gamma_4 = 2\theta_2 + \frac{1}{2}\theta_3 + \frac{1}{2}\theta_5$$

$$\gamma_5 = \frac{1}{2}\theta_3 + \frac{1}{2}\theta_5 \qquad \gamma_6 = 2\theta_2 + \frac{1}{2}\theta_3 + \frac{1}{2}\theta_5$$

$$\gamma_7 = \frac{1}{2}\theta_3 + \frac{1}{2}\theta_5 \qquad \gamma_8 = \frac{2}{3}\theta_2 + \frac{2}{3}\theta_4$$

$$\gamma_9 = \frac{1}{2}\theta_4 \qquad \gamma_{10} = \frac{1}{2}\theta_4$$

$$\gamma_{11} = \frac{2}{3}\theta_2 + \frac{1}{6}\theta_4 \qquad \gamma_{12} = \frac{2}{3}\theta_2 + \frac{1}{6}\theta_4$$

$$\gamma_{13} = \frac{2}{3}\theta_3 \qquad \gamma_{14} = -\frac{1}{3}\theta_3$$

$$\gamma_{15} = -\frac{1}{3}\theta_3 \qquad \gamma_{16} = \frac{1}{2}\theta_3$$

$$\gamma_{17} = \frac{1}{2}\theta_3 \qquad \gamma_{18} = \frac{1}{2}\theta_3$$

$$\gamma_{19} = \frac{1}{2}\theta_3 .$$

The coefficients ω_i and θ_i are given in Table A1.

Table A1 Coefficient in the Burnett equations

Coefficient	Maxwellian gas	Hard-sphere gas
ω_1	10/3	4.056
ω_2	2	2.208
ω_3	3	2.418
ω_4	0	0.681
ω_5	3	0.219
ω_6	8	7.424
θ_1	75/8	11.644
θ_2	-45/8	-5.822
θ_3	-3	-3.090
θ_4	3	2.418
θ_5	117/4	25.157